Power supply with parallel reactive and distortion power compensation and tunable inductive filter — Part 2

Michał GWÓŹDŹ, Rafał WOJCIECHOWSKI, and Łukasz CIEPLIŃSKI*

Poznan University of Technology, Faculty of Control, Robotics and Electrical Engineering, Piotrowo 3A, 60-965 Poznan, Poland

Abstract. The paper is the second part of the work, devoted to a DC power supply with a power factor correction function. The power supply is equipped additionally with a shunt active power filter function, which enables the compensation of reactive and distortion power, generated by loads, connected to the same power grid node. A tunable inductive filter, included at the input of the power electronics current source – the main block of the power supply – allows for an improvement of the quality of the system control, compared to the device with a fixed inductive filter. This improvement was possible by extending the current source "frequency response", which facilitated increasing the dynamics of current changes at the power supply input. The second part of the work briefly reminds the reader of the principle of operation and the structures of both the power supply control system and its power stage. The main purpose of this paper is to present the selected test results of the laboratory model of the electric system with the power supply.

Key words: distortion power; PFC; power supply; reactive power; tunable inductive filter.

1. INTRODUCTION

In the first part of the paper [1], the idea of the DC power supply (PSP) with the ability of active compensation of both reactive and distortion power was proposed. Moreover, thanks to extending the "frequency response" of the power electronics current source, which is a crucial part of the PSP, the quality of the compensation process was more efficient, compared to most of the typical solutions of active filters. The main purpose of this work is to present both the details of the PSP solution and the most important test results of the laboratory model of the electric system based on the PSP.

The following text is divided into four sections. In Sections 1, 2, and 3, the following issues are presented: the principle of operation of the PSP, details of the PSP power electronics and control sections, test results of the tunable inductive filter, and test results of the laboratory model of the power supply. The last part of the paper includes the conclusions.

2. STRUCTURE OF POWER SUPPLY

The general concept of power supply, based on the current source with the tunable inductive filter, was presented in the first part of the paper [1]. Therefore, only a brief description of the system structure and the basics of its operation is given here, for the reader's convenience.

The general block diagram of the electrical system, including the proposed power supply, cooperating with nonlinear loads,

connected to the same power grid node, is shown in Fig. 1. Compared to the diagram of the PSP, shown in the first part of the work, it is now more detailed. There is still an assumption that the entire system is powered from a 1-phase grid and the block denoted as the "OTHER LOADS" is not present there.
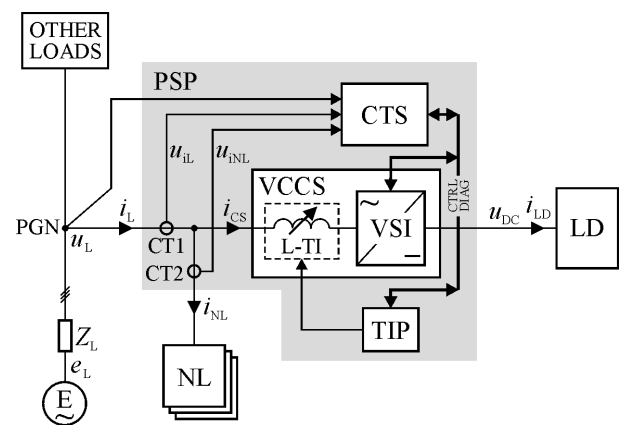

Fig. 1. Block diagram of the electrical system, including the power supply with compensation function

So, the system consists of the following basic components:
- E – power source.
- PGN – power grid node – with the internal impedance of the power grid, denoted as Z_L.
- PSP – power supply which is the subject of research; this is composed of the following: a power electronics voltage-controlled current source (VCCS), power stage, associated with the tuned inductor (TIP), and two current transducers (CT1, CT2). The CTS is the PSP control section, which is interconnected with both the voltage source inverter (VSI)

*e-mail: lukasz.cieplinski@put.poznan.pl

and the TIP – with the aid of the control and diagnostics lines (CTRL-DIAG).

- NL – a group of nonlinear loads, i.e., other devices connected to the same power grid node as the PSP.
- LD – a load of power supply, connected to its DC output circuit.

As a result of the compensation process, the total current drawn from the power grid node (i_L) should have both a suitable shape and a phase relation with the voltage in the power grid – depending on the compensation strategy [2–6]. In the case of this work, the power theory introduced by Fryze [6], was chosen for control of the compensation function of the device. In the light of this theory, the VCCS should generate at its input distorted current (i_{CS}) which, when combined with the current of nonlinear loads, results in a sinusoidal (theoretically) current, drawn from a grid. The operation of the PSP is, therefore, consistent with the PFC function [7].

2.1. Controlled current source

The controlled current source [7, 8], at the input of PSP, uses a voltage source inverter (VSI). In the physical implementation of the VSI, the IPM/IGBT type PM50RSA120, manufactured by MITSUBISHI ELECTRIC [9], was applied.
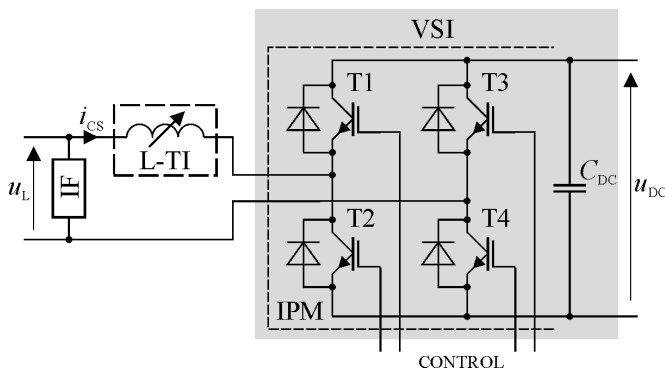

Fig. 2. Diagram of the power electronics stage of the power supply, associated with the controlled current source

The IF (input filter) block is the passive band-pass filter which allows for further minimization of ripples in the VCCS input current of the component, associated with the PWM.

2.2. Tunable inductive filter – simulation model studies

For the implementation of the tunable inductive filter, the phenomenon of the coupling of magnetic fluxes of two coils was applied – Fig. 3[1].
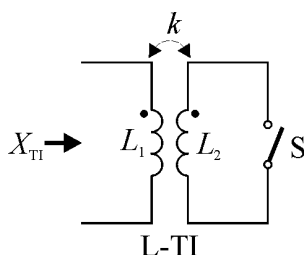

Fig. 3. Diagram of a tunable inductive filter implementation

The value of the equivalent reactance (X_{TI}) of the filter, seen from the power source side, reaches two values [1]:

$$X_{TI} = \left(1 - S_{T\text{-}TI}k^2\right)X\big|_{S_{T\text{-}TI}=0 \vee S_{T\text{-}TI}=1}, \qquad (1)$$

where: X – own reactance of L_1 and L_2 while $L_1 = L_2 = L$, k – magnetic coupling factor of coils, $S_{T\text{-}TI} = 0$ – S-switch is open, and $S_{T\text{-}TI} = 1$ – S-switch is closed.

The simulation studies, devoted to the details of the tunable filter implementation, were conducted in the Maxwell Environment. These showed that to achieve the assumed value of the equivalent inductance in both states of the switch, the sophisticated design of the magnetic circuit is necessary. As a result, the model of the inductor was based on a 3-winding transformer with a working air gap. For the purposes of modelling the construction of the considered inductor, the 3D field model was employed. In the elaborated model the material characteristics of the ferrite E-shapes (OT49928EC) with T-type ferrite material, manufactured by MAGNETICS Inc. [10], were used. The 3D view of the inductor construction, elaborated in Maxwell Software, and technical details of the inductor structure are shown in Fig. 4.
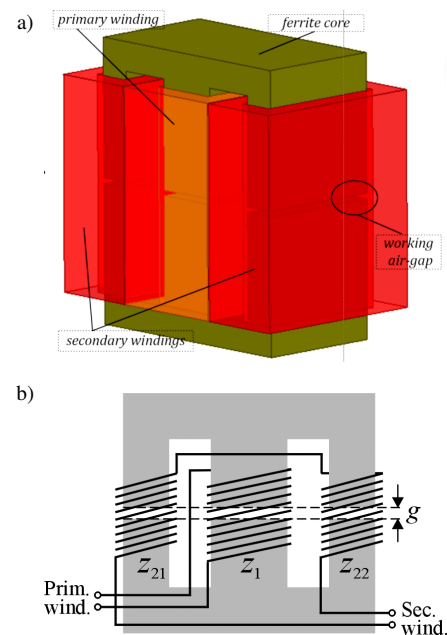

Fig. 4. 3D view of the model of a tuned inductor in Maxwell Environment (a) and details of the inductor structure (b)

In the work, the developed 3D field model of the inductor was used to determine the optimal values of the number of turns ($z_1 = z_{21} = z_{22} = z$) of the transformer windings (Fig. 4b) and the minimal value of the width (g) of the working air-gap, for which, the reactance ratio of the inductor

$$x_{S\text{-}TI} = \frac{X_{TI}\big|_{S_{T\text{-}TI}=0}}{X_{TI}\big|_{S_{T\text{-}TI}=1}}, \qquad (2)$$

should be close to 3, and the assumption is made that the value of the equivalent inductance (L_{TI}) should be in the range of 1–5 mH. These values were chosen because of the system simula-

2

Bull. Pol. Acad. Sci. Tech. Sci. 69(4) 2021, e137938

tion model studies with the PSP [1], as the compromise between a possible increase of the system dynamics and minimization of the PWM caused ripples, in the VCCS input current, in the system in the steady state.

To obtain the desired value of the ratio $x_{S\text{-}TI}$ in relation to the sought parameter values, i.e., the air-gap width and the turn number, the interval search method was used [11, 12], which was implemented in the optimization module of Maxwell Software. The method applied by the authors consists of searching for the best value of the objective function (here the appropriate value of the ratio $x_{S\text{-}TI}$) by systematically searching for the range of adopted values of parameters g and z. As a result of the optimization calculation, the value of the air-gap width $g = 2$ mm and the turn number value $z = 80$ was obtained. For such selected values of parameters, the inductance values in both states of the S were equal to 4.52 mH and 1.51 mH.

Based on the results of the simulation tests, the practical arrangement of the tuned inductor was possible. The details of this solution are presented in the next sub-section, devoted to the laboratory tests of the tunable inductor.

2.3. Tunable inductive filter – laboratory tests

The physical model of the inductor is shown in Fig. 5. In turn, in Fig. 6 the curves of L_{TI} vs. the width of the equivalent air-gap ($g_{eq} = 2g$, in relation to Fig. 4b) are presented, while the secondary winding was open and closed. The number of turns of the windings $z_1 = z_{21} = z_{22} = 80$.
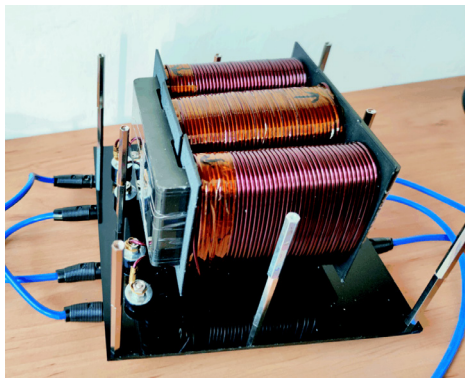

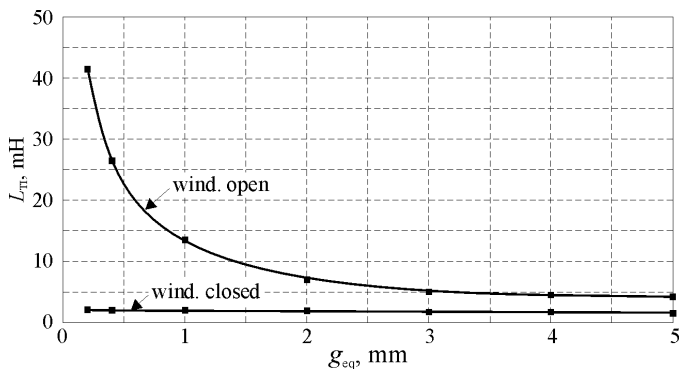**Fig. 5.** View of the laboratory model of the tuned inductor

Fig. 6. Curves of the equivalent inductance of the inductor vs. width of the equivalent airgap

As is visible, while the secondary windings are closed, the curve of equivalent inductance is practically flat in the entire range of the gap width value, which confirms the results of the simulation model tests. Based on these curves, the physical air-gap width, equal to 2.0 mm, was chosen.

Figure 7 depicts exemplary waveforms of the voltage powering the primary winding of the filter and the current associated with this voltage. Also, the saturation state of the magnetic core is visualized.
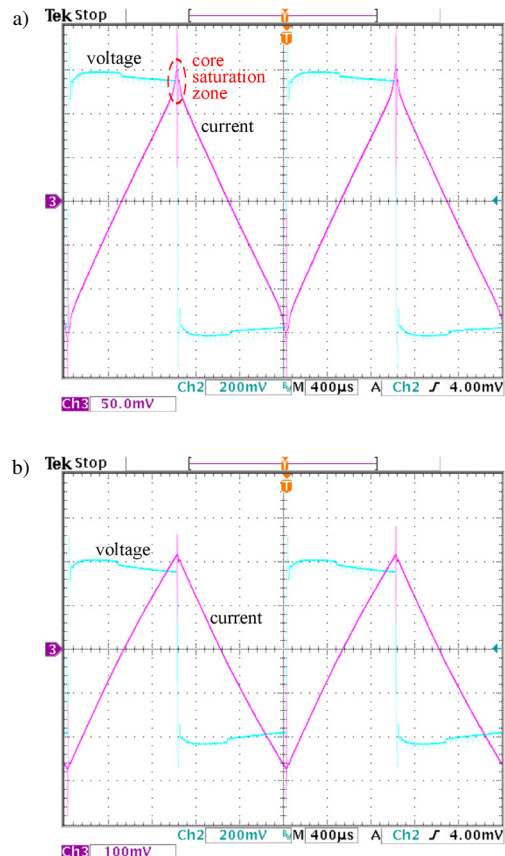

Fig. 7. Waveforms of voltage at the primary winding of the tuned inductor and primary current, while the secondary winding is open (a) and closed (b); vertical scale 40 V/div, 5 A/div (a), and 10 A/div (b)

Respecting the results of the laboratory tests, the summary of the technical parameters of the tuned inductor is as follows:
- Magnetic core: four E-shapes (OT49928EC) with T- type material, manufactured by MAGNETICS Inc.
- The number of turns $z_1 = z_{21} = z_{22} = 80$.
- Equivalent air gap width $g_{eq} = 4.0$ mm.
- Achieved inductance – in a quasi-linear range of the magnetic core operation: 4.52 mH with secondary winding open, and 1.51 mH with secondary winding closed.
- Winding resistance: 110 mΩ, primary, and 220 mΩ, secondary.
- The maximum magnitude of the primary current, in the quasi-linear range of the core operation: 13 A.

An inductive filter implementation in the PSP is shown in Fig. 8. This contains the TIP block that responds as the same block in Fig. 1.
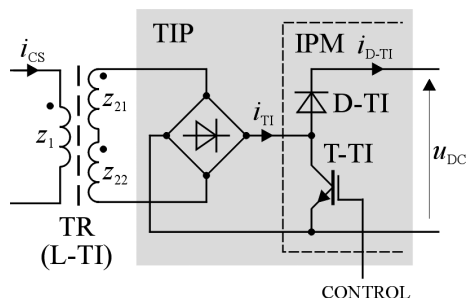
M. Gwóźdź, R. Wojciechowski, and Ł. Ciepliński

Fig. 8. Schematic diagram of the implementation of an inductive filter

In the role of the branch with T-TI and D-TI components, the third branch of the IPM is fulfilled.

3. PSP IMPLEMENTATION

The general view of the laboratory stand during tests is shown in Fig. 9.
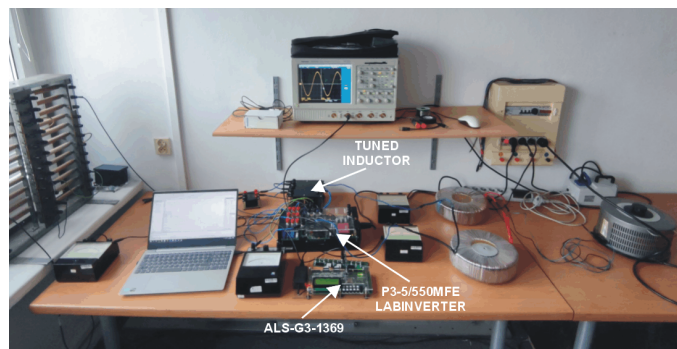

Fig. 9. General view of the laboratory stand

The control block in the laboratory prototype of the PSP was based on the ALS-G3-1369 Evaluation Board [13] with Analog Devices Inc. ADSP-21369 SHARC®, a 32-bit, floating-point, digital signal processor (DSP). This board is specialized for such power electronics applications, which require, among oth-

ers, the high computation power of a CPU and a high-precision PWM timing block. In the power stage of the PSP prototype, the P3-5-550MFE LABINVERTER was implemented [13]. This universal power electronics system was designed especially for advanced R&D applications.

In the following sub-sections, the details of PSP implementation, as well as selected results of laboratory experiments are described.

3.1. Structure of the PSP control system

The block diagram of the power supply control system is shown in Fig. 10. The right control algorithm consists of five main blocks, and each of these contains one to five internal sub-blocks. These blocks contain the individual parts of the algorithm and were implemented in software; these are shown on a grey background. The functionality of the main blocks and the role of the sub-blocks are described in the following sub-sections. All blocks were implemented on the platform – the ALS-G3-1369 Evaluation Board. This system is also equipped with multi-channel, 16-bit, ADC converters, with a simultaneous sampling capability, forming the input ports for the following external signals: u_L, u_{iL}, u_{iNL}, and u_{DC}. All internal digital signals in the CTS contain the prefix "s". The PWM timing block is denoted as the "PWM".

The PSP control algorithm was written in the C-language; the C/C++ Compiler, which is an integral part of VisualDSP++, is supported by the SIMD (Single Instruction Multiple Data) capability of the ADSP-213XX processors, which, in some conditions, doubles its computation power.

At the inputs of the selected blocks, decimation filters are implemented. Their main role is to reduce the signal sampling frequency, where possible, which allows for a reduction of the required computation power for the implementation of a given part of the algorithm. These filters are also described in the following sub-sections.

The basic parameters of the PSP laboratory model, as well as their values are listed in Table 1, which is included at the end of this section.
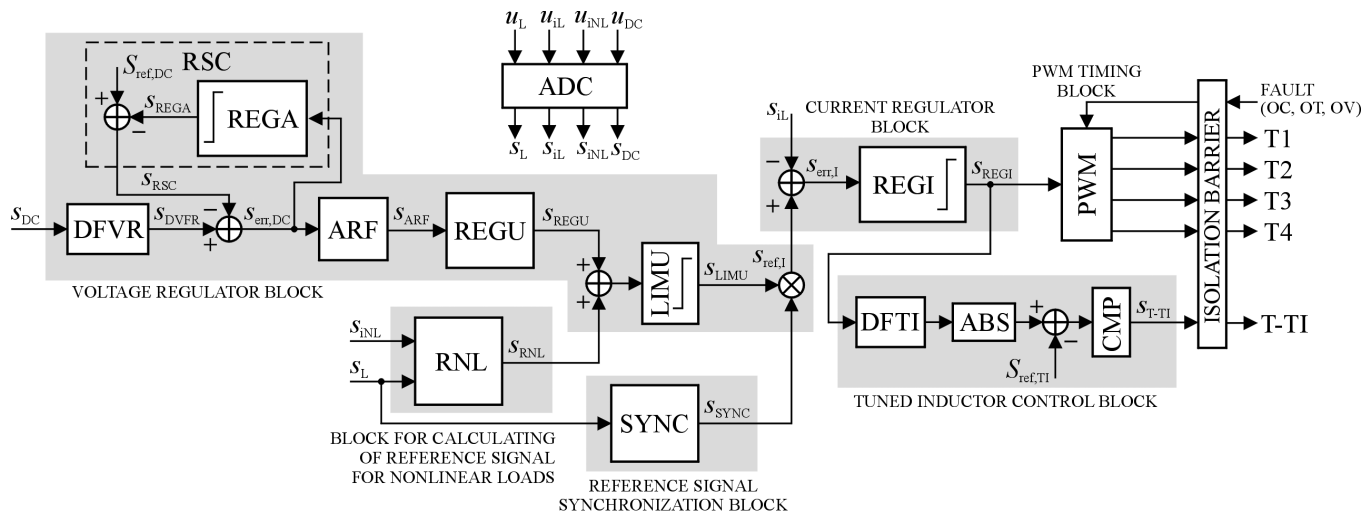

Fig. 10. The block diagram of the power supply control system (CTS)

4

Bull. Pol. Acad. Sci. Tech. Sci. 69(4) 2021, e137938

3.2. Block for calculating reference signal for nonlinear loads (RNL)

Both the structure and operating rules of the RNL block are associated with the "compensation" function of the power supply. The role of the block is to generate the signal (s_{RNL}), which is associated with the current value of the active power of the NL block. The value of this signal is calculated based on u_{L} and $u_{\text{iNL}} = r_{\text{CT2}}i_{\text{NL}}$, external signals, where r_{CT2} is the transfer ratio of the CT2. This signal is next summed with the voltage regulator output signal (s_{REGU}). So, this directly affects the amplitude of the reference signal ($s_{\text{ref,I}}$) for the current regulator block. The s_{RNL} waveform is a step function of the time, i.e., having a constant value in the half-period of the s_{SYNC} signal, which prevents strong distortion of the reference signal from the sinewave.

3.3. Reference signal synchronization block (SYNC)

The role of the SYNC block is to generate the sine-wave signal (s_{SYNC}) with a unity value amplitude, being in-phase with the voltage in the power grid node. The diagram of the SYNC block is shown in Fig. 11.
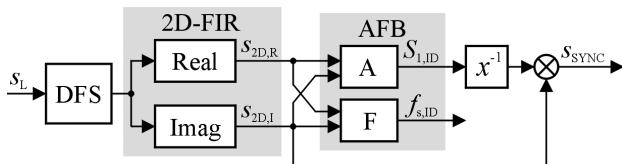

Fig. 11. Diagram of the reference signal synchronization block

The rules of operation of the main part of the SYNC block (i.e., DFS, 2D-FIR, and AFB) were presented, in detail, in the previous work [14]. So, only a brief description of this block operation is given in the following text.

The signal synchronization block consists of the following sub-blocks:

- DFS – decimation filter, with decimation factor (DF_{DFS}), currently equal to 8.
- 2D-FIR – the FIR filter, in which the magnitude part of transmittance is given by the following function:

$$|H_{\text{2D}}(f)| = \left[\frac{\sin\left(\pi \dfrac{(f - f_{\text{2D,0}})}{f_{\text{2D,0}}} \right)}{\pi \dfrac{(f - f_{\text{2D,0}})}{f_{\text{2D,0}}}} \right]^2, \qquad (3)$$

where: $f_{\text{2D,0}}$ is the filter centre frequency, which is currently set at 50 Hz.

The plot of (3) is shown in Fig. 12. This function provides a very effective filtration process of the input signal, in this case, the voltage in the power grid node, depending on the removal of higher harmonics, DC, and high-frequency components from this signal, while the value of the input delay is small. These properties are critical for the quality of the synchronization process, which should operate in real time.

The 2D-FIR generates a pair of signals – the orthogonal functions – $s_{\text{2D,I}}$, which is a sinusoidal function of the time, and
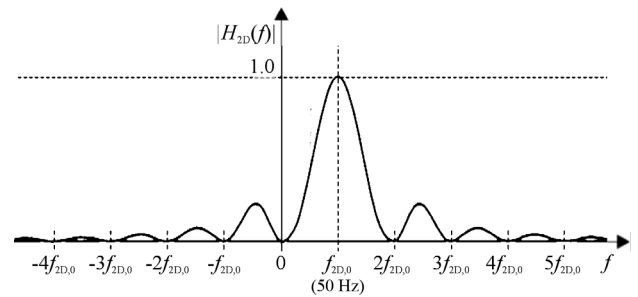

Fig. 12. The plot of the magnitude of the transmittance of the 2D-FIR

$s_{\text{2D,R}}$, which is a co-sinusoidal function of the time, in a particular case of $f_{\text{L}} = f_{\text{2D,0}}$, where f_{L} is the basic frequency of s_{L}. These signals are then processed in the AFB block.

- AFB – computes the frequency ($f_{\text{s,ID}}$) and amplitude ($S_{\text{1,ID}}$) of the basic harmonics of the u_{L}. The 2D-FIR output signal, $s_{\text{2D,I}}$, coming from its "Imag" sub-block, is in phase with u_{L}. The amplitude of this signal is then normalized by multiplying it by the output signal of the "x^{-1}" block, which computes the reciprocal value $S_{\text{1,ID}}$. As a result, the SYNC output signal has, at any time, a unity value of amplitude and is in phase with the basic harmonics of the voltage in the grid, i.e., $s_{\text{SYNC}}(t) = \sin(\omega_{\text{L}}t)$. This signal is next multiplied by the output signal of the voltage regulator (s_{LIMU}). As a result, the reference signal ($s_{\text{ref,I}}$) for the VCCS output current regulator is obtained: $s_{\text{ref,I}} = s_{\text{LIMU}}s_{\text{SYNC}}$. The selected signals in the SYNC block are shown in Fig. 13.
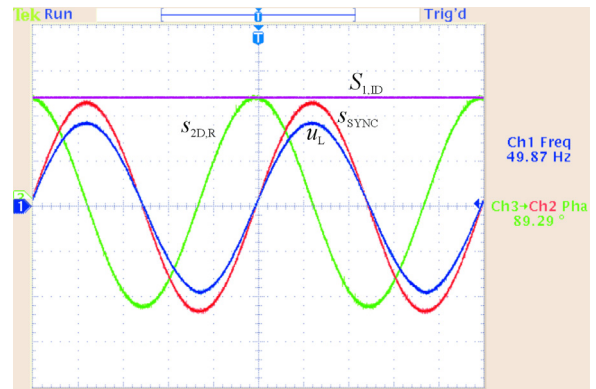

Fig. 13. Waveforms of the characteristic signals in the SYNC block as results of the laboratory tests

The laboratory tests showed that the operation of the SYNC block is very effective, e.g., the identification delay is no more than two periods of the input signal. The value of error related to the amplitude of s_{SYNC} was below 0.05%, while the phase error was in the range of ± 2 el. deg. – for typical conditions of the grid operation [15].

3.4. Voltage regulator block

This block is responsible for the control of the voltage in the DC circuit and contains the following sub-blocks:

- DFVR – decimation filter.
- ARF (Anti-Ripples Filter) – an FIR-type filter, whose role depends on both the elimination from the error signal, at the

input of the REGU ($s_{err,DC}$), the ripples, associated with the u_{DC} voltage and computing the true-average value of the DC voltage. In fact, these ripples are caused by the power grid voltage and could appear in the error signal ($s_{err,DC}$), since this operates, indirectly, at the u_{DC} voltage. In the case of the absence of the ARF block, the ripples in the error signal would strongly distort the reference signal for the current regulator ($s_{ref,I}$) from a sinewave. The magnitude part of the ARF transfer function is as follows [16]:

$$|H_{ARF}(f)| = \left| \cos\left(\frac{\pi}{2} \frac{f}{f_{ARF}} \right) \right|, \qquad (4)$$

where f_{ARF} is the filter characteristic frequency.

Currently, $f_{ARF} = 100$ Hz, which is double the voltage frequency in the power line. So, the zeros of (4) are set at 100, 300, and 500 Hz. The plot of this function, in the Nyquist band, is visualized in Fig. 14.
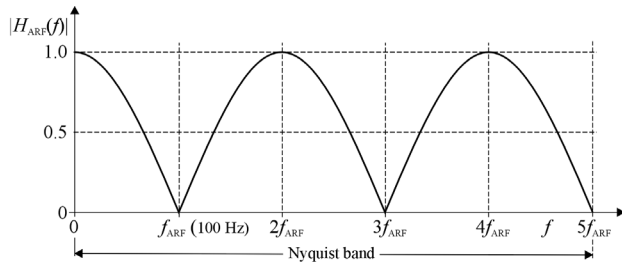

Fig. 14. The magnitude part of the ARF transfer function

- RSC – reference signal correction block. This block is one of the most important elements of the control algorithm. It operates on both the reference signal for the master voltage regulator (REGU), i.e., $S_{ref,DC}$, and the current value of the error signal ($s_{err,DC}$), associated with this regulator. The RSC output signal (s_{SRC}) is a value-corrected reference signal ($S_{ref,DC}$) for the REGU. The general idea of the RSC operation is based on work [17]. However, some essential differences appear.

The basic description of the RSC operation is given in the time-domain, which is, in this case, more convenient, compared to its description in the frequency-domain, and is as follows:

$$s_{RSC}(t) = S_{ref,DC} - s_{err,DC}(t) * h_{REGA}(t) =$$
$$= S_{ref,DC} - [s_{DVFR}(t) - s_{RSC}(t)] * h_{REGA}(t), \quad (5)$$

where $h_{REGA}(t)$ is the pulse response of the internal regulator (REGA) in the RSC and "*" is the symbol of convolution; $S_{ref,DC} = $ const.

By transforming (5) with respect to the feedback signal (s_{DVFR}), the following formula is obtained:

$$s_{DVFR}(t) * h_{REGA}(t) = S_{ref,DC} - s_{RSC}(t) +$$
$$+ s_{RSC}(t) * h_{REGA}(t). \qquad (6)$$

Assuming temporarily the simplest, i.e., the 0-order form of the REGA transfer function:

$$h_{REGA}(t) = \delta(t). \qquad (7)$$

Equation (6) now takes the following form:

$$s_{DVFR}(t) = S_{ref,DC}. \qquad (8)$$

Equation (8) means that the average value of the voltage in the DC circuit is equal to the reference signal, at any time. So, theoretically, the value of the control error is equal to zero. Nevertheless, these equations do not consider the impact of the RSC block operation on the stability of the entire control system. Hence, respecting the current value of the delays brought into the signal path of the voltage and current regulation blocks, the REGA was implemented as a 1st order low-pass filter. In such case, (8) takes the form:

$$s_{DVFR}(t) = S_{ref,DC}\left(1 - e^{-\frac{t}{\tau_{REGA}}}\right) \xrightarrow{t \to \infty} S_{ref,DC}. \qquad (9)$$

In other words, the value of the control error, in the steady state of the system, will theoretically be equal to zero.

- REGU – the regulator of the voltage in the DC circuit of the PSP. The REGU was chosen as the P-type one. This regulator operates on the error signal, $s_{err,DC}$. The REGU output signal (s_{REGU}) is then summed with the signal generated in the RNL block (s_{RNL}). The sum of both signals sets the amplitude of the reference signal for the current regulator.
- LIMU – the limiter of the voltage regulator output signal magnitude, imposing the maximum value of the current at the input of the current source – in the context of the current limitations of the real IGBT devices, as well as obtaining the operation of the tuned inductor in the quasi-linear range.

3.5. Current regulator block

This block is responsible for control of the VCCS input current. The main task of the regulator was to provide the LAG type [18] compensation of the system transfer function. The combination of P and PI topology, called "P2I" in the work, was chosen for the REGI block. However, this topology is different from the P-PI or PI-PI topologies that are presented in many studies, e.g., [19, 20]. The REGI transfer function, based on the P2I, is given by the following equation:

$$T_{REGI}(j\omega) = k_{I,0} \frac{j\dfrac{\omega}{\omega_{I,2}} + 1}{j\dfrac{\omega}{\omega_{I,1}} + 1}, \qquad (10)$$

where $k_{I,0}$ is the regulator gain, $\omega_{I,1}$, $\omega_{I,2}$ are the characteristic frequencies, and $\omega_{I,2} \gg \omega_{I,1}$.

The comparative plots of both parts of the transfer function for the P2I and PI types of the regulator are shown in Fig. 15. The gain value for a crucial frequency for PSP operation, i.e., 50 Hz, is comparable with the PI type of regulator. Above the characteristic frequency of $f_{I,1}$, both gain plots are very similar, while above the characteristic frequency of $f_{I,2}$ also the phase plots are comparable. As shown in this figure, the characteristic frequencies are in line with the actual transmittance of the REGI, implemented in the CTS.

The values of the regulator settings were determined based on the small-signal model of the VCCS [1] and the original program in C-Language, in which this model was applied.
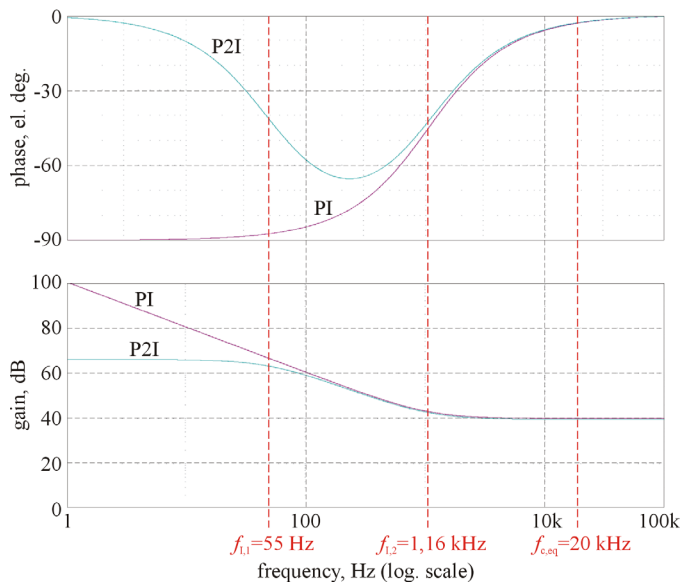
6

Bull. Pol. Acad. Sci. Tech. Sci. 69(4) 2021, e137938

Fig. 15. Magnitude and phase plots of the P2I and PI type regulator transfer function

The Nyquist criterion was used to evaluate the asymptotic stability of the VCCS.

In addition to the task of regulating the input current of the VCCS, another role of the REGI is to minimize the pulse modulation components (at the $f_{c,eq}$ frequency) in its output signal, the presence of which can lead to so-called "deterministic chaos" in the CTS, which would disturb the entire regulation process [21].

The REGI block is also equipped with a signal magnitude limiter at its output, which prevents the PWM block from entering an over-modulation state.

3.6. Tuned inductor control block (TIC)

The TIC block is responsible for generating the pulse-duration modulated signal ($s_{T\text{-}TI}$), which controls the T–TI switch, in the TIP block. This block consists of the following sub-blocks:

- DFTI – the decimation filter, which enables control of the width of the pulses in $s_{T\text{-}TI}$, i.e., a choice between the degree of minimization of the transient state in the VCCS input current and the value of the power losses in the elements of the TIP block. By design, the operating frequency of the power devices in the TIP block is much higher than in the other blocks of the PSP.
- ABS – block for calculating the absolute value of its input signal.
- CMP – the hysteresis comparator, which operates at the signal that is the difference of the ABS output signal and the reference signal for the TIC block ($S_{ref,TI}$) and generates the $s_{T\text{-}TI}$ signal.

3.7. Parameters of the PSP laboratory prototype

The parameters of the PSP laboratory prototype and their current values are listed in the following table. Only global parameters for the experiments are included. The values of some parameters had to be corrected, with respect to the simulation

model assumptions [1], to achieve the actual laboratory conditions. These corrections were related mainly to the tuned inductive filter and its control circuit.

Table 1
List of the basic parameters of the PSP prototype

No.	Parameter name	Parameter symbol (optional)	Parameter value
	General PSP parameters		
1	Nominal power grid voltage	–	230 V
2	Nominal DC output power	–	1.3 kW
3	Nominal DC voltage	–	450 V
4	Maximum magnitude of the PSP input current	–	13 A
5	Master sampling frequency in CTS	f_S	80 kHz
	VCCS power stage		
6	Tuned inductor equivalent inductance, S–switch open	L_{TI}	4.52 mH
7	Tuned inductor equivalent inductance, S–switch closed	L_{TI}	1.51 mH
8	Capacitance of the capacitor in DC circuit	C_{DC}	1 mF
9	PWM carrier frequency	–	10 kHz
	CTS – voltage regulator		
10	Decimation factor of DFVR	DF_{DFVR}	80
11	Gain of the REGU	$k_{U,0}$	0.3
12	Gain of the REGA	$k_{A,0}$	0.99
13	Characteristic time of the REGA	τ_{REGA}	10 ms
14	Signal clipping level in LIMA	$A_{L,A}$	±35 V
15	Reference signal magnitude in RSC	$S_{ref,DC}$	450 V
16	Signal clipping level in LIMU	$A_{L,U}$	±15 V
	CTS – current regulator		
17	Gain	$k_{I,0}$	2000 V/V
18	Characteristic frequency	$f_{I,1}$	55 Hz
19	Characteristic frequency	$f_{I,2}$	1.16 kHz
20	Signal clipping level	$A_{L,I}$	±450 V
	CTS – tuned inductor control block		
21	Decimation factor of DFTI	DF_{DFTI}	1
22	Reference signal magnitude	$S_{ref,TI}$	430 V

4. TESTS OF THE PSP LABORATORY MODEL

A set of experiments of the PSP and, mainly, its control algorithm were conducted using the "processor-in-the-loop" (PIL) modelling, among others. Most of the waveforms were obtained using the PLOT function of the VisualDSP++, which allows for graphic visualization of numerical data (typically, waveforms) stored in arrays [22].

As shown in the following figures, the most characteristic waveforms for the system operation were selected, while the NL block was the "thyristor voltage regulator" with a fire angle of 90 el. deg., loaded by the resistor. This kind of NL load places the highest demands on the dynamics of the compensation system. The DC output power was equal to the nominal one, while the power of the NL block was approx. 50% of the nominal PSP output power at the DC side. In the case of the waveforms in Fig. 16, the PSP compensation function was disabled.
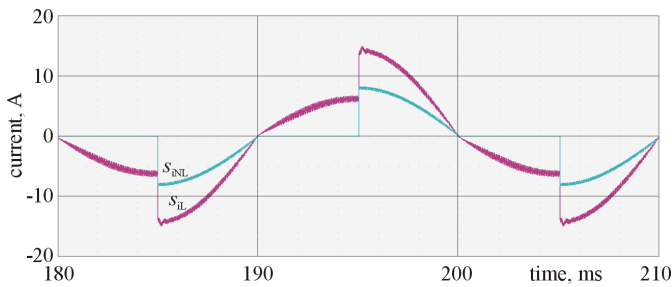
M. Gwóźdź, R. Wojciechowski, and Ł. Ciepliński

Fig. 16. Waveforms of the PSP input current and non-linear loads current while compensation function was disabled

Both kinds of inductive filters, i.e., fixed (Fig. 17) and tuned (Fig. 18), were respected, while the compensation function was activated. Fig. 18 also presents the waveforms of the REGI output signal and associated with this, the tuned inductor control signal $(s_{\text{T-TI}})$, in a transient state of the PSP input current.
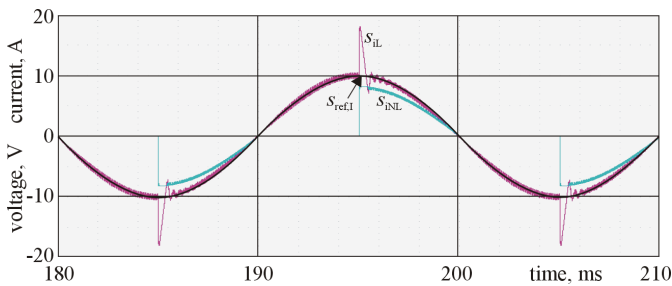

Fig. 17. Waveforms of the reference signal, the PSP input current, and non-linear loads current while the compensation function was enabled, and the fixed inductor was used

As the basic quantities characterizing the quality of the PSP compensation function operating, both the $TTHD$ of the i_{L} current and the duration of the transient state in this current (τ_{L}) were chosen. The following values of these quantities were obtained as results of the model tests:

- Power of the DC load equal to the nominal one
  - compensation function disabled, $TTHD = 29.5\%$,
  - compensation function enabled, with a fixed inductor, $TTHD = 13.4\%$, and with a tuned inductor, $TTHD = 9.0\%$.
- Power of the DC load equal to 17% of the nominal one
  - compensation function disabled, $TTHD = 52.5\%$,
  - compensation function enabled, with a fixed inductor, $TTHD = 23.5\%$, and with a tuned inductor, $TTHD = 15.5\%$.
- Duration of the transient state (averaged values)
  - fixed inductor, $\tau_{\text{L}} = 0.45$ ms,
  - tuned inductor, $\tau_{\text{L}} = 0.18$ ms.

The results obtained show approx. 1.5-times, according to the $TTHD$, and 2.5-times, according to τ_{L}, improvement, on average, in the input current quality, because of the PSP with the tuned inductor operating.

In turn, Fig. 19 shows the waveforms associated with the PSP response to step changes in the DC load.

In the steady state of the system, thanks to the RSC block operating, the average value of the DC voltage was close to the
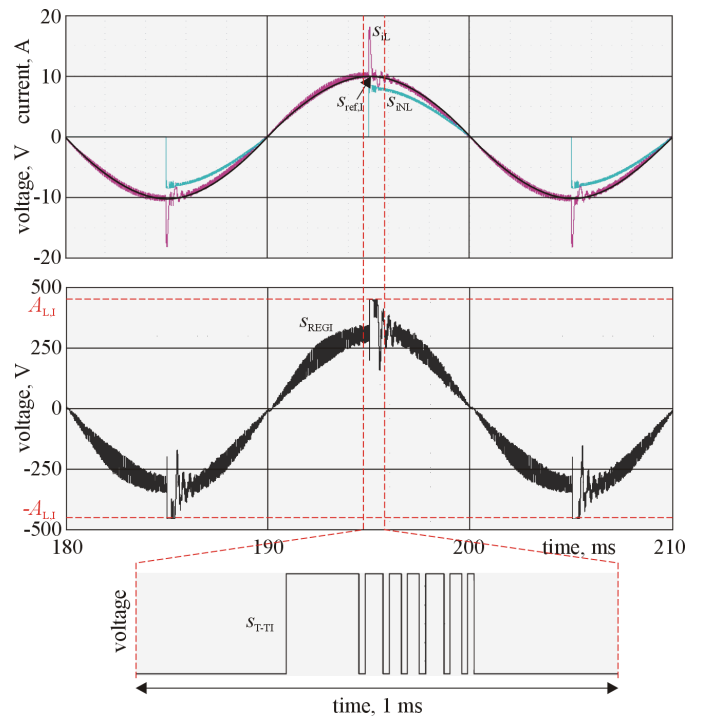

Fig. 18. Waveforms in the system while the compensation function was activated, and the tuned inductor was used. The following signals are presented: reference signal for REGI, PSP input current, non-linear loads current (upper figure), REGI output voltage (middle figure), and TIC block control signal (lower figure)
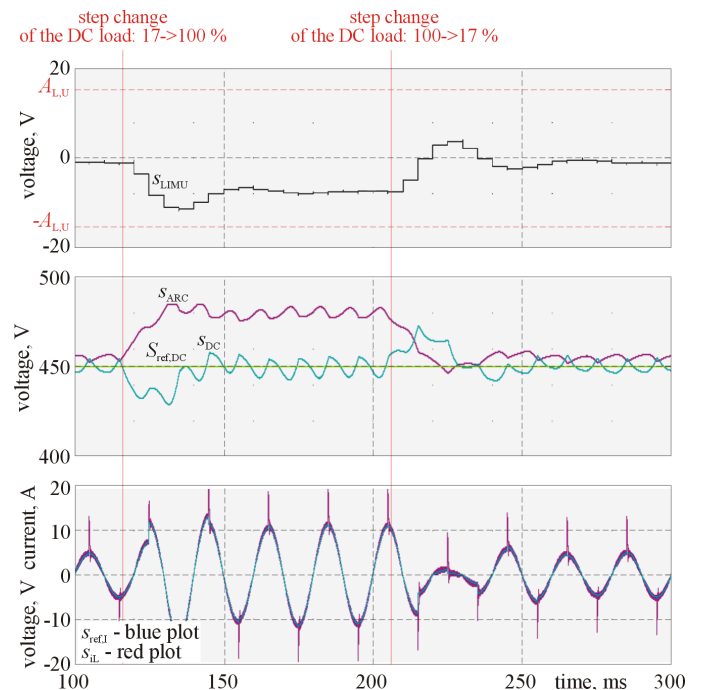

Fig. 19. Waveforms in the PSP as its response to step changes of the DC load

reference voltage; the value of the DC error was equal to approx. 1 V, i.e., 0.2% of $S_{\text{ref,DC}}$. The transient state after a step change of the DC load was equal to 2.5 periods of the line voltage, i.e., 50 ms.

8

Bull. Pol. Acad. Sci. Tech. Sci. 69(4) 2021, e137938

5. CONCLUSIONS

A set of experiments of an electric system with the power supply and its control algorithm, using the "processor-in-the-loop" (PIL) modelling, confirmed the effectiveness of its operation as a power supply, equipped with the additional function of a parallel active filter. However, the values of some parameters of the converter had to be corrected, in relation to its basic simulation model [1], to achieve the actual laboratory conditions – related mainly to the tunable inductive filter and its control circuit.

The laboratory tests showed that the operation of the reference signal synchronization block with the voltage in the power grid was also correct. The error related to the amplitude of this signal was below 0.05% while the phase error was in the range of ± 2 el. deg. – for normative conditions of the grid operation. The signal synchronization delay was no more than two periods of the power grid voltage.

The use of a tunable inductive filter facilitated a clear increase of the dynamics of the current changes at the power supply input – in relation to a system with a fixed value of this inductance. The results of tests of the PSP model indicate 1.5–2.5 times improvement, according to the criteria specified in the work, in the quality of the system operation, when a tunable filter was used. The implemented PSP control algorithm also made it possible to obtain the high quality of the regulation process of the DC voltage.

Considering a small degree of increase in the hardware complexity of this device, compared to the version without a compensation function, it seems that the proposed solution can be an economically attractive alternative for functionally specialized parallel active filters.

REFERENCES

[1] M. Gwóźdź, Ł. Ciepliński, and M. Krystkowiak, "Power supply with parallel reactive and distortion power compensation and tunable inductive filter – Part 1," *Bull. Pol. Acad. Sci. Tech. Sci.*, vol. 68, no. 3, pp. 401–408, 2020.

[2] Y. Ma, F. Hong, X. Zhou, and Z. Gao, "An overview on harmonic suppression," *2018 Chinese Control and Decision Conference (CCDC)*, Shenyang, 2018, pp. 4943– 4948, doi: 10.1109/CCDC.2018.8407987.

[3] M. Pasko, D. Buła, K. Dębowski, D. Grabowski, and M. Maciążek, "Selected methods for improving operating conditions of three-phase systems working in the presence of current and voltage deformation – part I," *Archives of Electrical Engineering*, vol. 67, no. 3, pp. 591–602, 2018.

[4] M. Siwczyński and M. Jaraczewski, "Reactive compensator synthesis in time-domain," *Bull. Pol. Acad. Sci. Tech. Sci.*, vol. 60, no. 1, pp. 119–124, 2012.

[5] D. Buła and M. Pasko, "Stability analysis of hybrid active power filter," *Bull. Pol. Acad. Sci. Tech. Sci.*, vol. 62, no. 2, pp. 279–286, 2014.

[6] S. Fryze, "Active, reactive, and apparent power in circuits with nonsinusoidal voltage and current", *Przegląd Elektrotechniczny*, vol. 13, pp. 193–203, 1931.

[7] M.H. Rashid, *Power Electronics Handbook*. Oxford, Elsevier, 2018.

[8] M. Krystkowiak, "Modified model of wideband power electronics controlled current source with output current modulation," *Elektronika*, vol. 57, no. 11, pp. 65–70, 2016 [in Polish].

[9] Mitsubishi Electric, *Intelligent Power Modules*. [Online]. Available: http://www.mitsubishielectric.com/semiconductors/products/powermod/intelligentpmod/index.html [Accessed: 05 Feb. 2021].

[10] Magnetics, [Online]. Available: https://www.mag-inc.com/home [Accessed: 05 Feb. 2021].

[11] S. Saeed, R. Georgious, and J. Garcia, "Modeling of magnetic elements including losses application to variable inductor", *Energies*, vol. 13, p. 1865, 2020, doi: 10.3390/en13081865.

[12] E. Chong, and S. Zak. *An Introduction to Optimization*. 4th ed. Wiley Publishing, 2013.

[13] Alfine-Tim [Online]. Available: http://analog.alfine.pl/oferta/produkty-alfine/systemy-uruchomieniowe [Accessed: 05 Feb. 2021].

[14] M. Gwóźdź, Ł. Ciepliński, and A. Gąsiorek. "Real-time identification of the selected parameters of periodic signals," *Progress in Applied Electrical Engineering, PAEE*, (on-line Conference), Kościelisko, Poland, 2020.

[15] Standard EN 50160 (2010) – Voltage characteristics of electricity supplied by public distribution networks.

[16] W. Kester, *The Data Conversion Handbook*. Newnes, Analog Devices Inc, 2005.

[17] S. Pop, D. Pitica, and I. Ciascai, "Adaptive algorithm for error correction from sensor measurement," *2008 31st International Spring Seminar on Electronics Technology*, Budapest, 2008, pp. 373–378, doi: 10.1109/ISSE.2008.5276632.

[18] J.C. Doyle, B.A. Francis, and A.R. Tannenbaum, *Feedback Control Theory*. Dover Publications, 2013.

[19] T. Żabiński and L. Trybus, "Tuning P-PI and PI-PI controllers for electrical servos," *Bull. Pol. Acad. Sci. Tech. Sci.*, vol. 58, no. 1, pp. 51–58, 2010.

[20] M. Naouar *et al.*, "FPGA-based speed control of synchronous machine using a P-PI controller," *2006 IEEE International Symposium on Industrial Electronics*, Montreal, QC, Canada, 2006, pp. 1527–1532, doi: 10.1109/ISIE.2006.295698.

[21] R. Porada and N. Mielczarek, "Modeling of chaotic systems in the ChaoPhS Program," in *Modelling Dynamics in Processes and Systems*, W. Mitkowski, J. Kacprzyk, (Eds). Studies in Computational Intelligence, vol. 180, Springer, Berlin, Heidelberg, 2009, doi: 10.1007/978-3-540-92203-2_1.

[22] Analog Devices, [Online]. Available: https://www.analog.com/en/products/adsp-21369.html#product-documentation [Accessed: 05 Feb. 2021].